Neurobiology of Aging 55 (2017) 177–189

Contents lists available at ScienceDirect

Neurobiology of Aging

journal homepage: www.elsevier.com/locate/neuaging

Amyloidosis and neurodegeneration result in distinct structural connectivity patterns in mild cognitive impairment

Thomas Jacquemont [a,b,c,d,e,f,*], Fabrizio De Vico Fallani [a,b,c,d,e], Anne Bertrand [a,b,c,d,e,g], Stéphane Epelbaum [a,b,c,d,h], Alexandre Routier [a,b,c,d,e], Bruno Dubois [a,b,c,d,h], Harald Hampel [a,b,c,d,h,i], Stanley Durrleman [a,b,c,d,e], Olivier Colliot [a,b,c,d,e,g,h,*], and the Alzheimer's Disease Neuroimaging Initiative

[a] Inserm, U1127, Paris, France
[b] CNRS, UMR 7225 ICM, Paris, France
[c] Sorbonne Universités, UPMC Univ Paris 06, UMR S 1127, Paris, France
[d] Institut du Cerveau et de la Moelle épinière, ICM, Paris, France
[e] Inria, Aramis project-team, Centre de Recherche de Paris, France
[f] Département de Biologie, Ecole normale supérieure, PSL Research University, F-75005, Paris, France
[g] Department of Neuroradiology, AP-HP, Hôpital de la Pitié-Salpêtrière, Paris, France
[h] Department of Neurology, AP-HP, Hôpital de la Pitié-Salpêtrière, Institut de la Mémoire et de la Maladie d'Alzheimer (IM2A), Paris, France
[i] AXA Research Fund & UPMC Chair, Paris, France

ARTICLE INFO

Article history:
Received 27 September 2016
Received in revised form 17 March 2017
Accepted 19 March 2017

Keywords:
Alzheimer's disease
MCI
Biomarkers
Structural connectome
Network analysis

ABSTRACT

Alzheimer's disease (AD) is increasingly considered as a disconnection syndrome. Previous studies of the structural connectome in early AD stages have focused on mild cognitive impaired subjects (MCI), considering them as a homogeneous group. We studied 168 subjects from the Alzheimer's Disease Neuroimaging Initiative database (116 MCI and 52 cognitively normal subjects). Biomarker-based stratification using amyloid biomarkers (AV45 PET) and neurodegeneration biomarkers (MRI and FDG PET) led to 4 subgroups based on amyloid positivity (A+/−) and neurodegeneration positivity (N+/−): A−N−, A+N−, A−N+, and A+N+. Using diffusion MRI, we showed that both MCI A−N+ and MCI A+N+ subjects displayed an alteration of the white matter in the fornix and a significant bihemispheric network of decreased connections. These network alterations in MCI A+N+ are stronger and more focal than those of MCI A−N+. Only MCI A+N+ subjects exhibited specific changes in hippocampal connectivity and an AD-like alteration pattern. Our results indicate that the connectome disintegration pattern of MCI subgroups differ with respect to brain amyloid and neurodegeneration. Each of these 2 AD biomarkers induces a connectome alteration that is maximal when they coexist.

1. Introduction

Alzheimer's disease (AD) is the most frequent age-related neurodegenerative disease and an exponentially growing health care problem (Ferri et al., 2005). As AD progresses, beta-amyloid and tau proteins accumulate in the brain, leading to inflammation, neuronal dysfunction, and cell death (Oddo et al., 2006). Neuronal loss results in macroscopic atrophy of the gray matter in neo and allocortical regions (Dubois et al., 2014; Ma et al., 2016). In addition to gray-matter atrophy, subcortical white matter is also progressively altered which results in the breakdown of anatomical connections between distant brain areas (Bartzokis, 2011; Braak and Braak, 1997; Braskie et al., 2011). In particular, previous neuroanatomical and neuropathological studies showed that, among the whole-brain connections, cortico-cortical connections and hippocampal circuits are specifically vulnerable to neurodegeneration early in the course of AD (Hof and Morrison, 1991; Hof et al., 1990; Morrison and Hof, 2002). The progress of neuroimaging techniques, in particular diffusion magnetic resonance imaging and functional MRI, as well as postprocessing (tractography) and network analysis methods, has enabled the in vivo study of the structural and functional connectivity that form the brain connectome. Connectomics has so far confirmed the impairment of

* Corresponding authors at: ICM–Brain and Spinal Cord Institute, Pitié-Salpêtrière, Hospital, 47-83, boulevard de l'Hôpital, 75651 Paris Cedex 13, France. Tel./fax: +33157274365.
E-mail addresses: t.jacquemont44@gmail.com (T. Jacquemont), olivier.colliot@upmc.fr (O. Colliot).

0197-4580/$ – see front matter © 2017 Elsevier Inc. All rights reserved.
http://dx.doi.org/10.1016/j.neurobiolaging.2017.03.023

network connectivity in AD observed by neuroanatomical and neuropathological studies, supporting the role of white-matter degeneration in the disease, and the fact that part of the symptoms is due to the disconnection of distant cortical regions (Daianu et al., 2013a,b; Fischer et al., 2015; Mallio et al., 2015; Nir et al., 2012, 2015; Prescott et al., 2014).

In AD, the pathological process begins decades before the onset of clinical dementia. Therefore, characterization of the preclinical and prodromal stages of AD is important for a better understanding of the disease and the design of new therapies. Numerous studies have focused on subjects with mild cognitive impairment (MCI) who present objective cognitive deficits but are not yet demented (Petersen, 2011; Petersen et al., 2009). Recently, several studies have studied the structural connectome based on diffusion MRI in subjects with MCI and have demonstrated impaired connectivity, similar to that observed in AD with a lower degree of severity (Daianu et al., 2013a,b; Mallio et al., 2015; Prescott et al., 2014).

In these studies, MCI has been considered as a homogeneous group representing one stage between cognitively normal (CN) and AD subjects. However, in the past years, the advent of different biomarkers has allowed researchers and clinicians to characterize AD at its earliest stages from a pathophysiological point of view. These indicators include biomarkers of β-amyloidosis (reductions in CSF $A\beta_{42}$ and increased amyloid PET tracer retention) and biomarkers of neuronal injury and neurodegeneration (increased CSF tau, decrease of fluorodeoxyglucose uptake on PET, structural MRI measures of hippocampal atrophy; Jack et al., 2010, 2013). Biomarkers have improved the characterization of the heterogeneity of the MCI phenotype by distinguishing patients with and without abnormal biomarkers of amyloidosis and neurodegeneration (Caroli et al., 2015; Petersen et al., 2013; Vos et al., 2015; Wisse et al., 2015). In particular, 2 subgroups of patients are of high interest. The first one is composed of patients with abnormal biomarkers of both amyloidosis and neurodegeneration (MCI A+N+, also called high likelihood MCI due to AD or prodromal AD). This population has been shown to display a high rate of APOE ε4 carriers, a greater cognitive decline over time and a higher rate of progression and conversion to AD (Caroli et al., 2015; Edmonds et al., 2015; Knopman et al., 2012; Prestia et al., 2013; Vos et al., 2013). The second group is that of patients who are amyloid negative but neurodegeneration positive, a group often referred to as MCI with suspected nonamyloid pathology (MCI SNAP) or MCI A−N+ (Jack et al., 2012, 2016b). Various studies have analyzed the differences between SNAP and amyloid positive patients, in terms of clinical and cognitive trajectories, APOE genotype, and underlying pathology (Caroli et al., 2015; Jack, 2014; Jack et al., 2010, 2014, 2016c; Knopman et al., 2012; Mormino et al., 2014; Petersen et al., 2013; Prestia et al., 2013; Toledo et al., 2014, 2015; Vos et al., 2013, 2015; Wirth et al., 2013; Wisse et al., 2015). For the moment, it is not known why this group differs from typical prodromal stages of AD with amyloidosis (MCI A+N+). Thus, because MCI is not a biologically homogeneous group and especially because MCI SNAPs may not be part of prodromal AD, MCI SNAPs may be a confounding factor in the results of connectomic studies in MCI.

The present work aims at studying the connectome of subjects with MCI, stratified according to their biomarker status, using diffusion-weighted magnetic resonance imaging (DWI), tractography and network analysis, and CN A−N− as control group. For this purpose, we analyzed DWI of 168 subjects from the ADNI database (116 MCI and 52 CN subjects). We first assessed the integrity of specific white-matter tracks combining diffusion tensor imaging scalar maps (including fractional anisotropy and mean diffusivity) and a white-matter atlas. Then, we reconstructed the whole-brain connectome of each patient using fiber tractography. Network analysis techniques were then applied to characterize the connectomes at global and local scales.

2. Materials and methods

2.1. Participants and image acquisition

Data used in the present study were extracted from the Alzheimer's Disease Neuroimaging Initiative (ADNI) database. The ADNI was launched in 2003 by the National Institute on Aging, the National Institute of Biomedical Imaging and Bioengineering, the US Food and Drug Administration, private pharmaceutical companies, and nonprofit organizations, as a $60-million, 5-year public-private partnership. The primary goal of ADNI has been to test whether serial magnetic resonance imaging, PET, other biological markers, and clinical and neuropsychological assessment can be combined to measure the progression of MCI and early AD. Determination of sensitive and specific markers of very early AD progression is intended to aid researchers and clinicians to develop new treatments and monitor their effectiveness, as well as lessen the time and cost of clinical trials. The principal investigator of this initiative is Michael W. Weiner, MD, VA Medical Center and University of California, San Francisco. ADNI is the result of efforts of many coinvestigators from a broad range of academic institutions, private corporations, and research participants have been recruited from >50 sites across the United States and Canada. The initial goal of ADNI was to recruit 800 adults but ADNI has been followed by ADNI-GO and ADNI-2. To date, these 3 protocols have recruited >1800 adults, ages 55–90 years, to participate in the research, consisting of cognitively normal older individuals, people with early or late MCI, and people with early AD. The follow-up duration of each group is specified in the protocols for ADNI-1, ADNI-2, and ADNI-GO. Research participants originally recruited for ADNI-1 and ADNI-GO had the option to be followed in ADNI-2. For up-to-date information, see www.adni-info.org.

Since the present work requires DWI data, only data from ADNI-GO and ADNI-2 were used since no DWI data were recorded in ADNI-1. Detailed inclusion and exclusion criteria of participants can be found in the ADNI-2 and ADNI-GO protocols. From the ADNI-GO and ADNI-2 databases, we selected all MCI and CN participants for which a T1-weighted scan (necessary for assessment of neurodegeneration and for connectome analysis), a DWI scan (necessary for connectome analysis), an FDG-PET scan (necessary for assessment of neurodegeneration), and an AV45-PET scan (necessary for assessment of amyloid status) at baseline were available. As a result, 168 participants were selected and entered into our study, 52 of them were CN and 116 of them were MCI. Moreover, in order to compute adjusted hippocampal volumes, we also selected all CN participants for whom a T1-weighted scan and for which both hippocampal volume and intracranial volume (ICV) were available. This resulted in 373 CN participants. Finally, to define biomarker cutoff values (AV45 standardized uptake value ratio [SUVr], normalized adjusted hippocampal volume and FDG SUVr), we selected, for each biomarker, AD participants who underwent the associated scan (respectively AV45-PET scan, T1-weighted scan, and FDG-PET scan). We obtained respectively for each biomarker 144, 275, and 243 AD participants.

MRI data were acquired as part of ADNI's procedures. All subjects underwent whole-brain MRI scanning on 3-Tesla GE Medical Systems scanners at 14 acquisition sites across North America. T1-weighted IR-FSPGR (spoiled gradient echo) anatomical scans were collected (256 × 256 matrix; voxel size = 1.2 × 1.0 × 1.0 mm^3; TI = 400 ms; TR = 6.98 ms; TE = 2.85 ms; flip angle = 11°), as well as diffusion-weighted images (DWI; 35 cm field of view, 128 × 128

acquired matrix, reconstructed to a 256 × 256 matrix; voxel size: 2.7 × 2.7 × 2.7 mm^3; scan time = 9 minutes). Forty-six separate images were acquired for each DWI scan: 5 T2-weighted images with no dedicated diffusion sensitization (b0 images) and 41 diffusion-weighted images (b = 1000 s/mm^2). This ADNI protocol was chosen after conducting a detailed comparison of several different DWI protocols, to optimize the signal-to-noise ratio in a fixed scan time (Jahanshad et al., 2010; Zhan et al., 2013). We visually checked all T1-weighted MR and DW images to exclude scans with excessive motion and/or artifacts; all scans were included.

2.2. Assessment of amyloid and neurodegeneration biomarkers

Assessment of amyloid and neurodegeneration biomarkers was made using readily available, processed data on the ADNI web site. Florbetapir F 18 (AV45) PET measures were obtained using standard methods, described in Landau et al. (2012). A composite SUVr for the florbetapir images was calculated by taking the mean SUVr of a set of regions typically associated with increased uptake in AD (frontal, anterior cingulate, precuneus, and parietal cortex), using gray matter of the cerebellum as reference region.

Neurodegeneration was assessed by both FDG-PET and MRI. FDG-PET measures were obtained using standard methods, also described in Landau et al. (2012). For FDG-PET analysis, SUVr was considered in a "meta region-of-interest" associated with hypometabolism in AD and was calculated as the mean of 5 regions (post cingulate gyrus, left and right angular gyrus and left and right temporal gyrus) using pons and vermis combined as a reference. Hippocampal volume and intracranial volume (ICV) were computed using the FreeSurfer suite. For each subject, we adjusted the raw hippocampal volume by his total ICV. To obtain a relative hippocampal volume change, we normalized the adjusted hippocampal volume by the expected volume of the hippocampus looking at the ICV. Normalized adjusted hippocampal volumes were obtained from the raw hippocampal volume using the following equation:

$$aHV_{norm} = \frac{HV - (a \times ICV + b)}{a \times ICV + b} \quad (1)$$

with aHV_{norm} the normalized adjusted hippocampal volume, HV the hippocampal volume, ICV the intracranial volume, a and b, respectively, the slope and intercept of the affine function representing the hippocampus volume in terms of the intracranial volume. We fitted a and b using data from 373 CN subjects.

2.3. Participants classification

To classify the participants based on amyloid and neurodegeneration markers, we chose the cut points for each imaging biomarker that corresponded to 90% sensitivity in clinically diagnosed patients with AD dementia from the ADNI database (Jack et al., 2012, 2016c; Knopman et al., 2012, 2013; Petersen et al., 2013; Wirth et al., 2013). For abnormal amyloid, we obtained a cut point for the AV45 PET composite normalized SUVr of 1.1 based on 144 clinically diagnosed patients with AD dementia. This threshold is consistent with already used threshold for this biomarker (Landau et al., 2012). Subjects with a higher or equal SUVr value were classified as amyloid positive (group A+), the other subjects as amyloid negative (group A−). For markers of neurodegeneration, subjects were classified as positive if they had a below threshold normalized adjusted hippocampal volume or abnormal FDG-PET hypometabolism. The 90% sensitivity cut point for the normalized hippocampal volume adjusted for total intracranial volume (aHV_{norm}) was −0.06 using volume data from 275 clinically diagnosed patients with AD dementia. This is interpreted as a hippocampal volume 6% below the expected hippocampal volume accounting for intracranial volume. For FDG-PET SUVr, the cutpoint value obtained was 1.27 using data from 243 clinically diagnosed patients with AD dementia. Subjects who displayed aHV_{norm} lower than or equal to −0.06 and/or an FDG-PET hypometabolism SUVr lower than or equal to 1.27 were defined as neurodegeneration positive (group N+), the other subjects were defined as neurodegeneration negative (group N−). Depending on those biomarkers, MCI patients were divided into 4 groups: A−N−, A+N−, A−N+, and A+N+ (see descriptive statistics of demographical data, Table 1). As a reference group for assessment of patients' connectome abnormalities, we defined a CN A−N− group composed of clinically normal participants with no abnormal biomarker.

2.4. T1-weighted image processing and brain parcellation

We processed T1-weighted images with the FreeSurfer suite (v5.3; Fischl et al., 2004), which provided nonuniformity and intensity correction, skull stripping, gray/white-matter segmentation, reconstruction of the cortical surface, and segmentation of cortical structures. The cortical ribbon was parcellated into 74 distinct regions per hemisphere based on the Destrieux atlas (Fischl et al., 2004). In total, with subcortical structures, 164 regions of interest were studied. We visually assessed FreeSurfer segmentations. No images were excluded.

2.5. Diffusion-weighted imaging (DWI) processing

For each subject, we aligned all raw DWI volumes to the average b0 image (DWI volume with no diffusion sensitization) using the FSL flirt tool with first 6 degrees of freedom (dof) allowing translations and rotations in 3D to correct for head motion and then 12 dof to correct for eddy current distortions. For each registration step, a normalized mutual information cost function was used. As recommended by Leemans and Jones (2009), the diffusion weighting directions were appropriately updated. To correct for echo-planar imaging–induced susceptibility artifacts, which can cause distortions at tissue-fluid interfaces, the skull-stripped b0 (nondiffusion-weighted) images were registered to the T1-weighted scans, first linearly using respectively FSL flirt tool with 6 dof and then nonlinearly using ANTs SyN algorithm (Avants et al., 2008). SyN is an inverse-consistent registration algorithm used with a mutual information cost function allowing echo-planar imaging–induced susceptibility artifacts correction (Leow et al., 2007). Then, we applied to the 41 DWI volumes the resulting linear transformation matrices and 3D deformation fields so that the DWIs and respective T1 images were in the same space. Finally, we corrected the DWIs for non-uniform intensity using the improved nonparametric nonuniform intensity normalization, ANTs N4 bias correction algorithm (Tustison and Avants, 2013). A single multiplicative bias field was estimated from the averaged b0 image, as suggested in Jeurissen et al. (2014), then the estimated bias field was applied to correct the intensity of all DW volumes. The implementation of the preprocessing was based on the Nipype toolbox. We visually assessed processed images for patient motion and distortion artifacts correction. No images were excluded from analysis because of excessive patient motion or distortion artifacts.

2.6. Fiber tractography

We performed whole-brain fiber tracking with the MRtrix software package (Brain Research Institute, Melbourne, Australia, Tournier et al., 2012). First, we fitted the diffusion tensors at each voxel to calculate fractional anisotropy (FA), mean diffusivity (MD), axial diffusivity (AxD), and radial diffusivity (RD) maps. Then, we computed the fiber orientation distribution (FOD) at highly

Table 1
Demographics of the studied participants

	MCI A−N−	MCI A+N−	MCI A+N+	MCI A−N+	CN A−N−
Number (%)	29 (25.4)	19 (16.7)	51 (44.7)	15 (13.2)	25
Age (std)	68.6 (6.8)[a,b,c]	69.8 (7.7)[d,e]	76.0 (6.1)[b,e,f]	74.0 (6.7)[a,d]	72.9 (4.8)[c,f]
Sex (%men)	21 (72.4)[a]	13 (68.4)	30 (58.8)	8 (53.3)[a]	14 (56.0)
Education (y)	16.8 (2.0)[b,g]	14.9 (3.0)[g,h]	15.5 (2.9)[b,f]	16.1 (6.7)	17.2 (2.8)[f,h]
MMSE (std)	28.7 (1.2)[b]	27.9 (1.9)	27.3 (1.7)[b,f]	28.0 (1.5)	28.9 (1.5)[f]
APOE ε4 positive (%)	11 (38.0)[b,c,g]	18 (94.7)[d,g,h]	45 (88.2)[b,f,i]	5 (33.3)[d,i]	5 (20.0)[c,f,h]

Means and standard deviations are displayed for continuous variables. Number is displayed for all categorical variables, with percentages within parentheses. Differences between groups were assessed using 2-tails Mann-Whitney *U* test for continuous data and χ^2 test for categorical variables. Significance level was set at $p < 0.05$.
Key: MCI, mild cognitive impairment.
[a] Significant difference between MCI A−N− and MCI A−N+.
[b] Significant difference between MCI A−N− and MCI A+N+.
[c] Significant difference between MCI A−N− and CN A−N−.
[d] Significant difference between MCI A+N− and MCI N A−N+.
[e] Significant difference between MCI A+N− and MCI N A+N+.
[f] Significant difference between MCI A+N+ and CN A−N−.
[g] Significant difference between MCI A−N− and MCI A+N−.
[h] Significant difference between MCI A+N− and CN A−N−.
[i] Significant difference between MCI A−N+ and MCI A+N+.

anisotropic voxels (FA >0.7) to determine the response function, which we used for constrained spherical deconvolution to accurately estimate the FOD (Tournier et al., 2007). We then generated fibers with a probabilistic tracking algorithm that samples FOD at each step. The algorithm generated 150,000 fibers of minimum length 20 mm. Default tracking parameters included a step size of 0.2 mm, minimum radius of curvature of 1 mm and FOD cutoff of 0.1. All voxels in the 1-mm dilated white-matter mask were used as seeds and the tracking procedure was stopped if a fiber reached a voxel outside the mask or if a stopping criterion was met (high fiber curvature or low FOD). Finally, to reduce the biases in quantitative measures of connectivity introduced by the streamlines reconstruction method and to improve biological accuracy of our structural connectome, we applied the spherical-deconvolution informed filtering of tractograms approach (Smith et al., 2013). We visually assessed streamlines for each patient for correct tractography, 2 patients from the MCI A+N− category were excluded because of incorrect B0 brain segmentation.

2.7. Computation of structural networks

Topological changes in the brain's networks may be analyzed using graph theory. In such analyses, the brain network is represented as a graph, that is, a set of units (called "nodes") and a set of lines linking the nodes together (called "links"). The network's nodes are typically defined as cortical and subcortical gray-matter regions, while the edges correspond to the white-matter connections between those regions. In our study, the graph is composed of 164 nodes that correspond to the cortical and subcortical regions. For any pair of nodes i and j, representing distinct anatomical regions i and j, an edge was added to G if at least one fiber tract connected these 2 anatomical regions (Hagmann et al., 2008). In DWI studies, a given edge is weighted by a measure of the "strength" of the connectivity between the 2 corresponding nodes. In our case, the edge was weighted by the fiber density between the 2 regions, defined as the number of fibers connecting the 2 regions normalized by the surface of the regions (Hagmann et al., 2008):

$$A_{i,j} = \frac{2}{S_i + S_j} |F_{i,j}| \quad (2)$$

where i and j are the indices of 2 different regions (i and j ranging from 1 to 164), $|F_{i,j}|$ is the number of fibers connecting region i to region j and S_i (respectively S_j) is the surface of region i (respectively region j). For subcortical structures, S corresponds to the volume of the region. We refer to the weight associated with the edge as the connectivity strength.

2.8. Structural connectome analysis

To analyze subjects' structural connectomes, we performed 3 different types of analyses.

2.8.1. Integrity of anatomical white-matter tracks

We assessed the integrity of a set of anatomical white-matter tracks defined in the DTI-81 white-matter atlas (Hua et al., 2008; Wakana et al., 2007). The DTI-81 Atlas is a stereotaxic probabilistic white-matter atlas that fuses DTI-based white-matter information with an anatomical template (ICBM-152). The warping of this atlas to each individual patient provides a parcellation of the white matter of the patient into anatomical tracks. The integrity of the tracks was assessed by analyzing the average FA, MD, AxD, and RD in each track. To that purpose, each scalar map of each patient was put into correspondence with the DTI-81 Atlas space by coregistering it to the FA map template with ANTs SyN algorithm (Avants et al., 2008). Then for each subject, the mean scalar value in each tract was computed.

2.8.2. Network-based statistics

We assessed global differences in interconnected network components between groups with network-based statistics (NBS, Zalesky et al., 2010). This analysis looks at the topological organization of the statistically more impaired connections by considering them as a module. In other words, NBS identifies altered connections and gathers them in a module to study the significance of these alterations at the scale of the module. Thus, the highlighted impairment should not be interpreted at the scale of individual connections, but at the scale of the whole module itself. Specifically, the procedure assesses if the size of the module is significantly larger than the ones observed randomly. The size of a module can be defined as the number of connections in this module (referred to as "extent"). The extent only takes into account the width of the module without looking at the strength of the alterations within the module. In addition to the extent of the module, we also examined the strength of alterations in each module by computing the sum of the opposed logarithm of the *t*-test of each connection in this cluster (referred to as "log"). The log size, as the extent size, takes into account the width of the module (because logarithms are

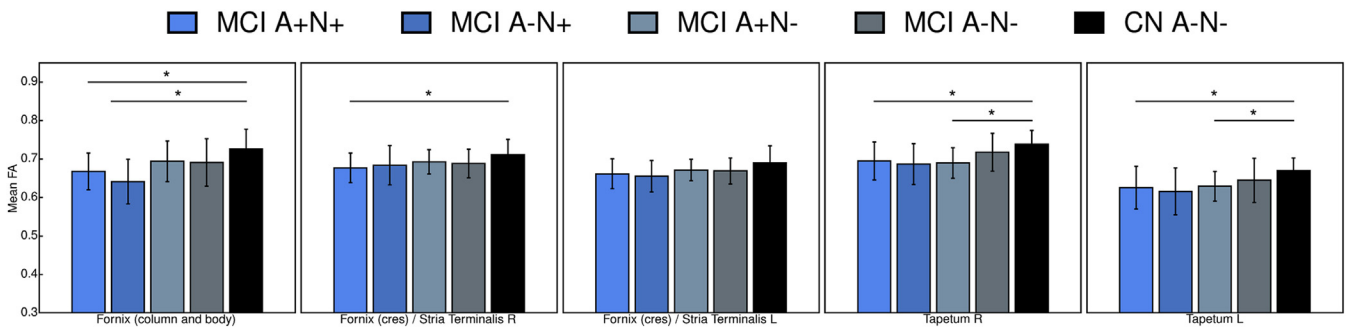

Fig. 1. Mean FA in anatomical white-matter tracks. Mean FA values for the fornix and the tapetum for which significant differences were found. The bar graph shows mean values (and standard deviation) for each group. $^{*}p < 0.05$ for Mann-Whitney *U* test. Abbreviations: FA, fractional anisotropy; L, left; MCI, mild cognitive impairment; R, right.

summed over each connection of the module) but also the strength of the alteration (because each connection in the module is weighted by the opposed logarithm of the associated *t*-test).

2.8.3. Graph analysis

Properties of brain networks can then be examined by analysis of the topology of the corresponding graph (Hagmann et al., 2008; Rubinov and Sporns, 2010). The graph structure (i.e., the organization of its links) can be analyzed by computing several indices (or metrics) corresponding to different topological properties. We used the Brain Connectivity Toolbox to calculate the indices (Rubinov and Sporns, 2010). The indices we computed can be roughly grouped into: (1) local metrics that characterize the nodes of graph and (2) global metrics that characterize the graph as a whole (De Vico Fallani et al., 2014). The local metrics were: node degree (number of links connected to a node), strength (sum of the weight of all links connected to a node), local efficiency (average inverse shortest path length in a node neighborhood) and clustering coefficient (the fraction of a node's neighbors that are neighbors of each other). The global metrics were: mean degree (mean node degree over the network), mean strength (mean node strength over the network), global efficiency (inverse of the harmonic mean of the shortest path length between each pair of nodes within the network), clustering coefficient (mean clustering coefficient over the network), characteristic path length (mean across the network of the minimum number of links necessary to travel from one node to another in the network) and small-worldness reflecting the tendency of the network to exhibit both shortcuts (integration) and clustering connections (segregation).

2.9. Statistical analysis

We used a general linear model to regress out the age, the sex, and the number of years of education effect from our variables of interest. Specifically, our variables of interest were the mean FA, MD, AxD, and RD for each tract in the tract integrity analysis, each edge weight of the graphs in network-based statistics and the different computed graph indices in our topological analysis.

2.9.1. Integrity of anatomical white-matter tracks

For each DTI scalar in each tract of the atlas, significant mean scalar changes between groups were assessed using a 2-tails Mann-Whitney *U* test. Correction for multiple comparisons was performed using the false discovery rate procedure.

2.9.2. Network-based statistics

We performed NBS following the sequence: (1) mean connectivity strength changes were calculated with 1 tail Student *t*-test at each connection; (2) network edges that survived a *p*-value lower than 0.01 uncorrected were retained; and (3) the size of the largest cluster was calculated. The statistical significance of the initial largest cluster size was estimated with a permutation test procedure: groups were randomly shuffled, and then the largest cluster size null-distribution was obtained by repeating steps 1, 2, and 3. The null-distribution was created using 50,000 permutations. Note that while the choice of the NBS threshold for the *p*-value is arbitrary, it can affect only sensitivity and not specificity (Zalesky et al., 2012).

2.9.3. Graph analysis

Node clustering coefficient, node efficiency, network characteristic path length, network clustering coefficient, and network efficiency metrics were normalized by dividing the metric by the mean metric value of 100 matched random networks (mean degree is preserved). Significant node and networks metrics change between groups were calculated using a 2-tails Mann-Whitney *U* test. Correction for multiple comparisons was performed using the false discovery rate procedure.

3. Results

3.1. Integrity of anatomical white-matter tracks

We found a significant decrease of FA in the column and the body of fornix of MCI A+N+ and MCI A−N+ compared with CN A−N− (Fig. 1). MCI A+N+ group also displayed a significant decrease of FA in the right fornix cres (posterior pillars, Fig. 1). MCI A+N− and MCI A+N+ displayed a significant decrease of FA in the tapetum bilaterally compared with CN A−N− (Fig. 1). No significant differences were found between MCI A+N+, MCI A−N+ and MCI A+N−. Moreover, no differences were found in any of the other tracts. Results for all tracts are shown in the Supplementary Fig. S1. Consistent with the FA analysis, compared with CN A−N−, MCI A+N+ group displayed a significant increase of MD in the column and the body of the fornix, the right fornix cres and the tapetum bilaterally. Moreover, MCI A+N+ also displayed a significant increase of MD compared with CN A−N− in the body and the splenium of the corpus callosum, the right superior fronto-occipital fasciculus, the hippocampal part of the cingulum bilaterally and the superior corona radiata bilaterally (Fig. 2). Similarly, consistent with the FA analysis, MCI A−N+ group displayed a significant increase of MD compared with CN A−N− in the column and the body of the fornix. Still compared with CN A−N−, MCI A+N+ also displayed a significant increase of MD in the right fornix cres, the body of the corpus callosum, the left superior corona radiata, the superior fronto-occipital fasciculus bilaterally, the hippocampal part of the cingulum bilaterally, and the right tapetum (Fig. 2). Finally, the MCI A+N− group displayed a significant increase of MD compared with

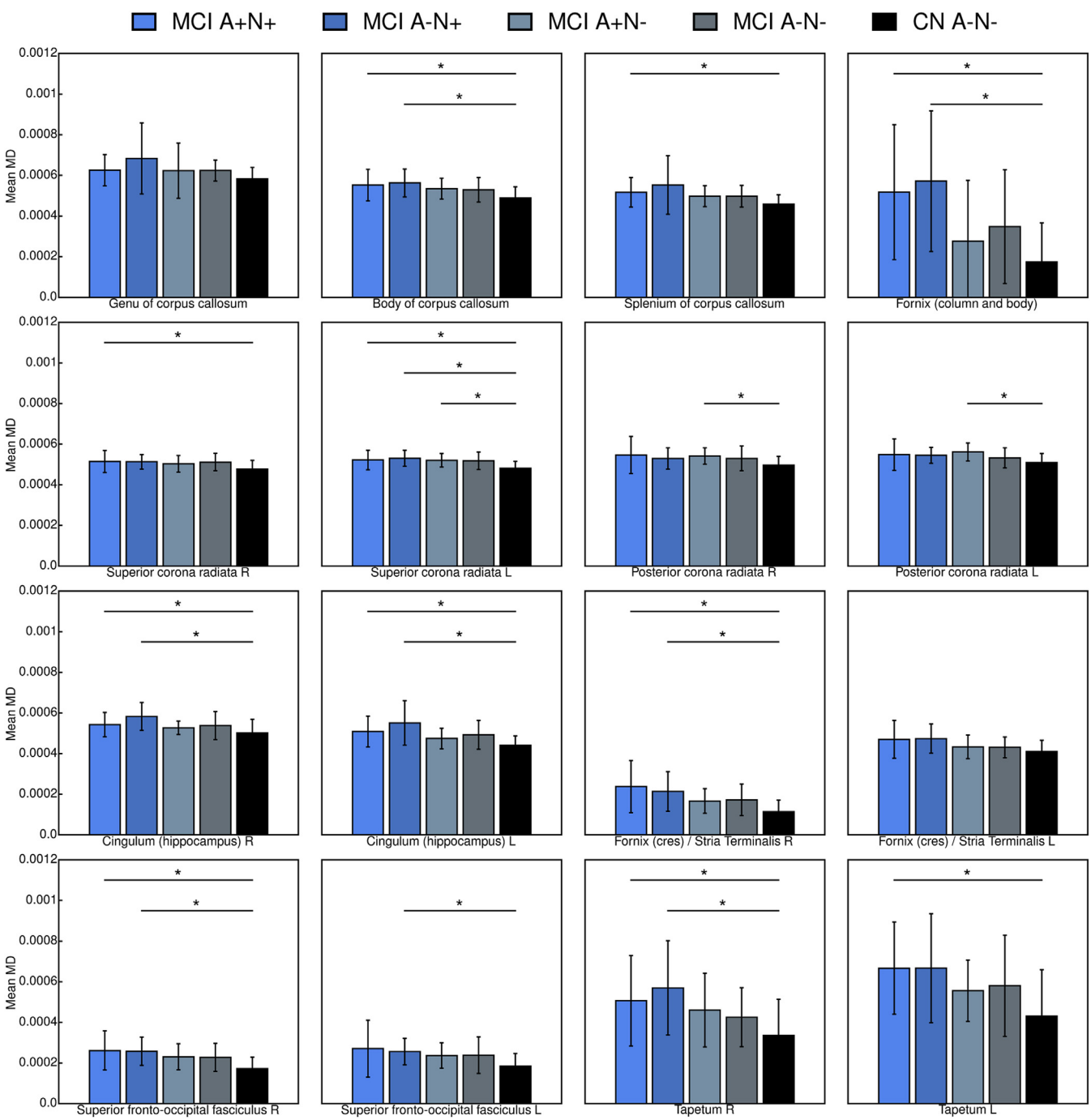

Fig. 2. Mean MD in anatomical white-matter tracks. Mean MD values for the corpus callosum, the fornix, the superior and posterior corona radiata, the hippocampus part of the cingulum, the superior fronto-occipital fasciculus and the tapetum for which significant differences were found. The bar graph shows mean values (and standard deviation) for each group. $^{*}p < 0.05$ for Mann-Whitney *U* test. Abbreviations: L, left; MD, mean diffusivity; R, right.

CN A−N− in the left superior corona radiata and the posterior corona radiata bilaterally (Fig. 2). No differences were found in any of the other tracts (results for MD for all tracts are shown in Supplementary Fig. S2). Results for both AxD and RD for all tracts are shown in the Supplementary Figs. S3 and S4, respectively and were consistent with the altered tracts observed with FA and MD.

3.2. Network-based statistics

Using network-based statistics (Zalesky et al., 2010), we found a significantly impaired module for MCI A+N+, MCI A−N+ and MCI A−N− compared with CN A−N− (Table 2). Network-based statistics also unveiled significantly impaired modules between MCI subgroups (Fig. 3). We found an impaired module of 63 disconnections between 56 nodes in MCI A+N+ compared with MCI A−N− ($p = 0.008$, Fig. 3A). The most impaired region was the left caudate nucleus with 11 disconnections followed by the right caudate nucleus with 8 disconnections. This module is a bihemispheric network with 36 disconnections in the left hemisphere (57%), 19 disconnections in the right hemisphere (30%), and 8 interhemispheric disconnections (13%). We also found an impaired module in MCI A−N+ of 216 disconnections between 131 nodes compared with

Table 2
Characteristics of impaired modules in MCI A+N+, MCI A−N+, and MCI A−N− compared with CN A−N−

	MCI A+N+	MCI A−N+	MCI A−N−
Number of disconnections	24	160	74
Number of nodes	20	113	53
%Connections: LH−RH−InterH	96−0−4	27−39−34	42−28−30
%Connections: basal−cortical−CB	0−87.5−12.5	1−86−13	0−90−10
Most disconnected area	L G Temporal middle	R Cerebellum	L G oc temp med Lingual R G oc temp med Lingual
Nb of disconnection	7	14	8
p-value			
Extent	0.04	0.046	0.024
Log	0.037	0.049	0.021

We indicate the number of nodes in the module to assess the extent of the module compared with that of the whole network (formed by 164 nodes). We also indicate the lateralization of the module (percentage of disconnections) in the left hemisphere only (LH), the right hemisphere only (RH), and interhemispheric connections (interH), and the percentage of baso-basal disconnections (Basal), cortico-cortical disconnections (Cortical), and cortico-basal disconnections (CB). Finally, we indicate the most disconnected area for each comparison along with the associated number of disconnections. *p*-values were computed using network-based statistics.
Key: CB, cortico-basal; G; gyrus; H, hemisphere; L, left; MCI, mild cognitive impairment; R, right.

MCI A−N− ($p = 0.008$, Fig. 3B). This module is also a bihemispheric network with 61 disconnections in the left hemisphere (28%), 102 disconnections in the right hemisphere (47%), and 53 interhemispheric disconnections (26%). The most impaired region was the right cerebellum with 20 disconnections. No significant module was found comparing MCI A−N+ to MCI A+N+ (MCI A+N+ > MCI A−N+, $p > 0.05$). We then looked at the strength of these modules by using the log size (sum of the opposed logarithm of the *t*-test of each connection in the module). Interestingly, when taking into account the strength of the alterations using the log size, the impaired module in MCI A−N+ compared with MCI A−N− failed to reach the significance ($p > 0.05$), whereas the impaired module in MCI A+N+ compared with MCI A−N− stayed significant ($p = 0.009$). By comparing MCI A+N− to other MCI subgroups and CN A−N−, no significantly altered module was observed. Results are summarized in Supplementary Table S2.

3.3. Structural connectome topology analysis

Consistent with previous studies on topological properties of the brain connectome, our networks displayed a small world topology (small-worldness values $\sigma_{CN\_A-N-} = 1.74$, $\sigma_{MCI\_A-N-} = 1.78$, $\sigma_{MCI\_A-N+} = 1.82$, $\sigma_{MCI\_A+N+} = 1.76 > 1$; Sporns et al., 2000). We did not find significant change of any of the global network metrics in MCI A+N+, MCI A−N+, MCI A+N−, and MCI A−N− compared with CN A−N− or between MCI subgroups (Supplementary Fig. S5). For local node metrics, we found a significant increase of node normalized clustering coefficient in MCI A+N+ compared with MCI A−N− in 4 structures (Fig. 4): left hippocampus, right hippocampus, right amygdala, and right nucleus accumbens. Mean values and standard deviations are summarized in the Supplementary Table S3. This difference in the left hippocampus was also associated with an increase of normalized local efficiency

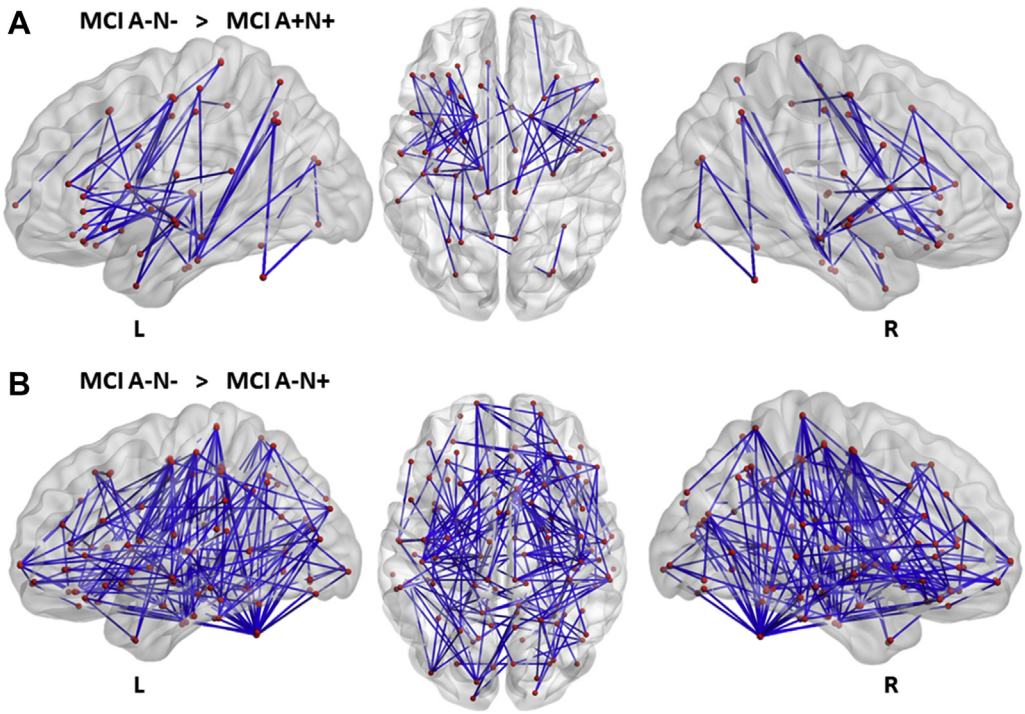

Fig. 3. Network-based analysis of MCI A+N+ and MCI A−N+ compared with MCI A−N−. Significant modules of impaired connection were found both in MCI A+N+ and MCI A−N+ compared with MCI A−N−. A larger module was found in MCI A−N+ and a smaller one in MCI A+N+. (A) Module impaired in MCI A+N+ compared with MCI A−N−. This cluster is formed by 63 disconnections and 56 nodes, $p = 0.008$. (B) Module impaired in MCI A−N+ compared with MCI A−N−. This cluster is formed by 216 disconnections and 131 nodes, $p = 0.04$. Abbreviation: MCI, mild cognitive impairment.

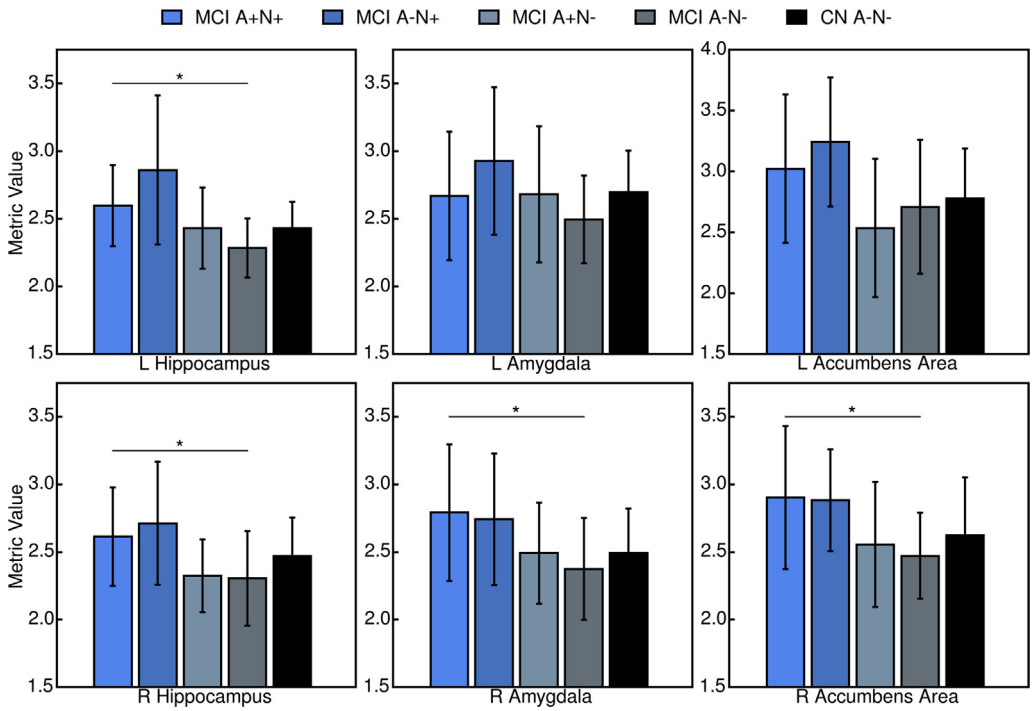

Fig. 4. Nodes normalized clustering coefficient. Significant differences were found in patients with MCI A+N+ compared with MCI A−N− in 4 structures: left hippocampus, right hippocampus, right amygdala, and right nucleus accumbens. Bar height represents the mean metric value, and the error bar represents one standard deviation from the mean. $^{*}p < 0.05$ for Mann-Whitney *U* test. Abbreviations: L, left; MCI, mild cognitive impairment; R, right.

(Supplementary Fig. S6). No significant changes were observed for MCI A−N+ and MCI A+N− compared with MCI A−N−.

4. Discussion

In this study, we used DTI scalars, tractography, and graph theory to study the structural connectome in subgroups of MCI subjects stratified by amyloid and neurodegeneration biomarkers. We demonstrated differences and similarities in network alterations depending on biomarker profile. In particular, MCI A+N+ and MCI A−N+ displayed alterations of the fornix and of the hippocampal part of the cingulum. Moreover, MCI A+N+ exhibited stronger and more focal connectivity alterations with a hippocampal clustering coefficient increase, whereas MCI A−N+ were associated with less severe but more diffuse network abnormalities.

4.1. Biomarker-based stratification of MCI patients

By performing a biomarker-based stratification of MCI patients in the ADNI-GO and ADNI-2 cohorts, we found that 25.4% of MCI patients were negative for both amyloid and neurodegeneration biomarkers, 16.7% were positive for only the amyloid biomarker, 44.7% were positive for both, and 13.2% were positive for only the neurodegeneration biomarkers. This distribution is consistent with previous studies (Caroli et al., 2015; Petersen et al., 2013; Prestia et al., 2013; Wisse et al., 2015). To further understand the nature of the neurodegeneration, we investigated the distribution of biomarkers subgroups based on whether neurodegeneration was achieved by hippocampal volume (HV) alone, FDG-PET alone, or both modalities (Supplementary Table S4). Of all MCI A+N+, 21.5% were positive for HV alone, 31.5% were positive for FDG PET alone, and 47% were positive for both biomarkers. Of all MCI A−N+, 46.7% were positive for HV alone, 33.3% were positive for FDG PET alone and 20% were positive for both biomarkers.

4.2. MCI patients positive for both biomarkers of amyloid and neurodegeneration

MCI A+N+ subgroup, which fits with the current model of prodromal AD, displayed the most impaired connectome (Jack et al., 2010, 2013). Using FA, MD, AxD, and RD to analyze the integrity of anatomical white-matter tracks, we showed for each DTI scalar that MCI A+N+ displayed an early alteration of the white matter in the fornix (columns and body and right crus of the fornix; these structures are shown in the Supplementary Fig. S7). The fornix belongs to the Papez circuit, is known to play an important role in memory and has been shown to be impaired in AD (Caso et al., 2015; Delano-Wood et al., 2012; Laxton et al., 2010; Mayo et al., 2017; Molinuevo et al., 2014; Nowrangi and Rosenberg, 2015; Wisse et al., 2015). Thus, in agreement with previous studies, we showed that the breakdown of the fornix and the hippocampal part of the cingulum happens at an early phase of AD, at the MCI A+N+ stage (Metzler-Baddeley et al., 2012). This alteration of the Papez circuit is consistent with the observed increase of MD, AxD, and RD in the hippocampal part of the cingulum (bilaterally for MD and only on the left for AxD and RD). Moreover, this breakdown of the Papez circuit was linked to a specific increase of nodal clustering coefficient affecting the left and right hippocampi in MCI A+N+ compared with MCI A−N−. To our knowledge, these are the first results showing that the connectomes of MCI subgroups are not equivalent, and that biomarker positive groups display specific connectome changes as compared with MCI subjects with normal biomarkers. This is consistent with reported hippocampus connectivity data, specifically the fact that the main efferent fibers of the hippocampus are collected in the fornix and connect the hippocampus to subcortical brain regions (Daitz and Powell, 1954; Knowles and Schwartzkroin, 1981; Tamamaki et al., 1988). It should be noted that previous studies have shown a global increase in clustering coefficient in AD dementia patients, as compared with

CN individuals (Daianu et al., 2013b; He et al., 2008; Yao et al., 2010). Here, we showed that such an increase in clustering is present at the local scale since the prodromal stage. This early and specific alteration of hippocampus local topology is consistent with previous neuroanatomical and neuropathological studies showing that hippocampus circuits are particularly vulnerable to the AD neurodegeneration process (Morrison and Hof, 1997, 2002). The clustering coefficient represents the fraction of a node's neighbors that are connected together. Thereby, the increase of the clustering coefficient of a node reflects the increment of interconnectivity among the nodes' neighborhood. This can occur either because of an increase in connectivity within the neighborhood, or because of a decrease in connectivity with remote nodes that are weakly connected to the neighborhood (Bollobás, 1998). Thus, the observed rise of the clustering coefficient of the hippocampi for the MCI A+N+ group can be interpreted as the result of long-range disconnections which tend to isolate the hippocampi and their high-connected neighborhoods. This is consistent with the non-alteration of left and right hippocampi nodal strength and degree we observed in our study. Indeed, it demonstrates that this is more the specific alteration of long-range connections than the number of disconnections itself which results in an alteration of both hippocampi clustering coefficient. Both the observed fornix alterations and increase in hippocampal clustering coefficient may be interpreted as a network analysis signature of the typical neurofibrillary degeneration progression during AD, which extend in a stereotypical sequence from the hippocampal region toward remotely connected areas (Braak and Braak, 1997).

Consistent with previous studies, MD, AxD, and RD appeared to be more sensitive than FA for the detection of white-matter microstructural changes (Acosta-Cabronero et al., 2010; Metzler-Baddeley et al., 2012). By looking at MD and AxD DTI scalars, we highlighted changes in white-matter integrity in superior and posterior corona radiata in MCI A+N+. Moreover, looking at MD, AxD, and RD, we also highlighted an alteration of the superior fronto-occipital fasciculus bilaterally. Although they are not well explained by the specific neurodegeneration process, these alterations of corona radiata and superior-occipital fasciculus have already been reported in previous studies (Gold et al., 2014; Mayo et al., 2017; Meng et al., 2012; Molinuevo et al., 2014). Because these alterations were also displayed by MCI A−N+ and MCI A+N− subgroups (but not by MCI A−N−), we hypothesized that these mild white-matter alterations without associated FA decrease were more linked to a small nonspecific neurodegeneration process, rather than a specific AD-linked neurodegeneration process.

Using network-based statistics, we found significantly impaired clusters in MCI A+N+ compared to MCI A−N− and CN A−N−. In MCI A+N+ compared with CN A−N−, the most disconnected area within the cluster was the left middle temporal gyrus with 7 disconnections over the 24 disconnections of the module. These disconnections are very interesting because previous study has shown that middle temporal gray-matter atrophy predicts decline to AD in MCI patients (Korolev et al., 2016). Here, we show that, during the progression of the disease, middle temporal connectivity is also early and specifically affected in MCI A+N+. In MCI A+N+ compared with MCI A−N−, the most disconnected area within the cluster was the left caudate nucleus. Because the caudate nucleus is a subcortical structure and so does not form large white-matter tracks, we hypothesized that this connectivity alteration could reflect a local disconnected state, and not the alteration of specific tracks link to the progression of the AD in these patients. The same mechanism could explain the observed increase of the normalized clustering coefficient in the right accumbens area.

We also observed an increase of the clustering coefficient for the right amygdala in MCI A+N+. This alteration of amygdala is consistent with previous studies showing that the amygdala is also affected at the very early stage of AD (Eustache et al., 2016; Poulin et al., 2011). Here, we showed that the MCI A+N+ group already displays an alteration of local amygdala connection topology.

At the global scale, MCI A+N+ did not significantly differ from CN A−N−. These results are consistent with a prior study showing that, whereas AD patients display global topological alterations, the topology of subjects with MCI is closer to that of CN individuals (Daianu et al., 2013b). This nodal clustering coefficient alteration without significant global changes is consistent with the idea that, at the prodromal phase, AD-related lesions slowly progress from the hippocampus to the whole cortex (Braak and Braak, 1997).

In addition, using each DTI scalar (FA, MD, AxD, and RD), the MCI A+N+ subgroup displayed an early and very specific bilateral alteration of the tapetum (these structures are shown in the Supplementary Fig. S8A). Interestingly, the tapetum is formed by the splenium fibers of the corpus callosum where we found a significant alteration of MD and RD (in both splenium and body of the corpus callosum). Moreover, the tapetum is also a small area of tracks crossing as shown in the Supplementary Fig. S8B. Near to the tapetum cross the posterior thalamic radiations and the superior longitudinal fasciculus which are 2 altered tracks in AD (Madhavan et al., 2015; Zhu et al., 2015). Thus, because tapetum is not specifically altered in amyloid negative MCI subgroups and because Aβ oligomers are known to impair long-range connections, we hypothesized that these alterations could be due to Aβ progression in these patients and that the tapetum integrity could be seen as a marker of AD Aβ injury within the brain (Warren et al., 2013).

Finally, with the alteration of the Papez circuit and tapetum neighboring tracks' white matter, the increase of hippocampal and amygdala clustering coefficient and the disconnection of the middle temporal gyrus, MCI A+N+ was the only MCI subgroup to display a typical AD-like disconnection pattern. Our results suggest that connectome studies in MCI would strongly benefit from a stratification of patients according to amyloid and neurodegeneration biomarkers.

4.3. MCI patients positive for amyloid only

Previous study showed that MCI A+N− subgroup displays cognitive impairments despite lack of obvious neurodegeneration (Wisse et al., 2015). Using NBS, network scale indices, and node scale indices, we did not highlight significant cluster impairment or connectome topological changes in MCI A+N− compared with CN A−N− or others MCI subgroups. In particular, MCI A+N− did not display alteration of the fornix, showing that even though fornix alterations have been described at the MCI stage, they are not present in all MCI patients (Madhavan et al., 2015; Metzler-Baddeley et al., 2012). Longitudinal studies of MCI A+N− connectome are needed to follow the progression of MCI A+N− connectome alterations and see whether subjects with MCI A+N− will develop an alteration of the fornix and the hippocampus connectivity (as MCI A+N+) or will have a different alteration pattern. But interestingly, as for MCI A+N+, MCI A+N− displayed a significant alteration in the tapetum FA bilaterally. Opposed to MD, RD, and AD, FA is directly related to white-matter integrity and sensitive to microstructural alterations (Alexander et al., 2011). This result confirms the specificity of tapetum white-matter integrity alteration in amyloid positive MCI subgroups. MCI A+N− is a conflicting and a not well-characterized category. Previous studies have shown that MCI A+N− group seems intermediate between MCI A+N+ and MCI A−N− in term of conversion rate and cognitive deterioration, but discrepancies appear between studies (Caroli et al., 2015; Petersen et al., 2013; Vos et al., 2015; Wisse et al., 2015). Our study is consistent with this prior knowledge, showing that

MCI A+N− white matter is less altered than MCI A+N+ but more altered than MCI A−N.

4.4. MCI patients positive for neurodegeneration only (MCI SNAP)

Looking at FA, MD, AxD, and RD, MCI A−N+, as MCI A+N+, displayed a fornix alteration (column and body of the fornix only for FA and both column and body of the fornix and right fornix cres for MD, AxD, and RD; shown in the Supplementary Fig. S7). Moreover, as MCI A+N+, MCI A−N+ displayed an increase of MD in the hippocampal part of the cingulum. These fornix and cingulum alterations appeared to be specific to neurodegeneration positive MCI subgroups and could be explained in MCI A−N+ by the way we defined the neurodegeneration in our study. Because the neurodegeneration positivity is partly defined by the hippocampus degeneration, it is not surprising to observe both fornix and cingulum degeneration in the neurodegeneration-positive MCI population. Indeed, among MCI A−N+ patients, 66.7% of them were positive for aHV_{norm} (Supplementary Table S4). Nevertheless, opposed to MCI A+N+, these fornix and cingulum alterations were not strong enough to alter hippocampal connectivity topology. This result is consistent with the wide cluster of disconnections we observed using NBS (e.g., 216 disconnections gathering 131 nodes when comparing MCI A−N+ to MCI A−N−). Using the extent size, this wide module was significantly impaired ($p = 0.04$), suggesting extended white-matter alterations, while, when taking into account the strength of the alterations using the log size, this wide module failed to reach significance ($p > 0.05$), showing that this module is formed by barely impaired connections, insufficient to impair hippocampal connectivity topology. These weak alterations on MCI A−N+ network could explain the observed increase of MD in the body of the corpus callosum and the right tapetum without any significant FA changes, suggesting minor white-matter integrity alterations. These wide but weak changes in connectivity suggest diffuse and diverse underlying neurodegeneration processes, rather than specific white-matter microstructural changes. Knopman et al. highlighted that MCI A−N+ lacked of specific longitudinal volumetric and metabolic decline profile, which is consistent with our results suggesting more diffuse and nonspecific network abnormalities resulting in a lack of connectome topological alteration profile in MCI A−N+ (Knopman et al., 2015). Interestingly, using NBS and comparing MCI A−N+ to both MCI A−N− and CN A−N−, the most impaired area was the right cerebellum with respectively 20 and 14 disconnections. The presence, among MCI A−N+ of subjects with altered cerebellum connectivity could be explained by cerebrovascular disease able to affect cerebellum connections, but this is probably not the only explanation. Moreover in these 2 impaired clusters cerebellum disconnections represents only 9% of the whole disconnections of the clusters. Thus the cerebellum does not seem to be a characteristic impaired area in MCI A−N+.

Finally, this more diffuse but weaker pattern of degeneration is likely to reflect the heterogeneity of MCI A−N+ etiology. The presence of different pathological processes (such as isolated tauopathy, early lewy body disease, hippocampal sclerosis, vascular changes), with different topologies over the brain within the same group, may explain the observed wider but weaker degeneration pattern of MCI A−N+ (Jack et al., 2016b). In accordance with this hypothesis of heterogeneity of MCI A−N+ etiologies, we found that among all MCI A−N+, only 20% were positive by both biomarkers, whereas they were 47% in the MCI A+N+ (Supplementary Table S4). However, it has been also proposed that MCI A−N+ may reflect a proportion of AD individuals with subthreshold Aß SUVr (Vos et al., 2015, 2016). We investigated if MCI A−N+ subgroup displayed significant higher AV45 SUVr compared with others amyloid negative subgroups (MCI A−N− and CN A−N−; Supplementary Fig. S9). We did not find a specific increase of AV45 SUVr in MCI A−N+ compared with MCI A−N− or CN A−N−. This is consistent with previous study showing no significant increase of florbetapir SUVr in MCI A−N+ classified using CSF $A\beta_{42}$ as amyloid biomarker (Wisse et al., 2015). Our results support the hypothesis that the degeneration processes at play in MCI A−N+ and MCI A+N+ are of different nature, which is one of the hypotheses proposed to explain the origin of MCI A−N+ (Jack, 2014; Jack et al., 2013, 2016b; Knopman et al., 2015; Wisse et al., 2015).

4.5. MCI patients negative for both biomarkers of amyloid and neurodegeneration

MCI A−N− (also called low-AD likelihood group) is an interesting group of patients with MCI but without any proof amyloid pathology or neurodegeneration (Albert et al., 2011). This group was the less impaired group without any white-matter alterations and no connectomes topology changes compared with CN A−N−. However, using NBS, we observed a significantly impaired cluster comparing to CN A−N−, and the most impaired areas were the medial occipito-temporal gyrus and lingual gyrus bilaterally, with 6 disconnections. Interestingly, this area is implied in memorizing (particularly visual inputs), working memory and is working jointly with hippocampus during problem-solving tasks at least in children (Cho et al., 2012; Kozlovskiy et al., 2014). The specific and bilateral disconnection of this area could explain the observed cognitive impairment without amyloid or neurodegeneration processes. In the MCI A+N+ subgroup, we observed a significant increase in normalized clustering coefficient when compared with MCI A−N−, but this increase was not significant when compared with CN A−N−. To explain this unexpected result, we hypothesized that 2 mechanisms coexist: an increase of clustering coefficient in MCI A+N+, due to specific AD-linked long-range disconnections; and a decrease of clustering coefficient in MCI A−N−, due to nonspecific short-range disconnections. This hypothesis is coherent with the observed changes in the 5 groups (Fig. 4). It suggests that connectomic analysis can help distinguishing neurodegenerative diseases based on their targets, that is, long-range or short-range networks, as they would cause opposite changes in clustering coefficients.

4.6. Limitations

The main limitation of this work is the relatively small size of the cohort, particularly of the MCI A−N+ and MCI A+N− subgroups (respectively 15 and 19 patients). This may have led to reduced statistical power to detect differences between groups, and it is possible that additional alterations would be discovered within a larger cohort. Another limitation is that our biomarker-based stratification model did not use the very recently published unbiased A/T/N classification scheme incorporating tau biomarkers (T; Jack et al., 2016a). We did not incorporate tau biomarkers in our classification because tau PET imaging was not available in our data set, and CSF tau was available only in a small fraction of the patients. However, the A/N classification scheme is consistent with that of previous studies distinguishing between MCI patients. Nevertheless, future studies using the A/T/N scheme would be particularly useful to disentangle the specific contribution of tau to structural network alterations. It can be noted that our diagnostic groups display significant differences in ages, with MCI A+N+ and MCI A−N+ groups being significantly older than MCI A−N−, and MCI A+N−. This is consistent with previous work on subjects with MCI showing that MCI A+N+ and MCI A−N+ are characteristic of an older population (Petersen et al., 2013; Wisse et al., 2015). Age

and years of education have been shown to have a significant impact on white-matter microstructure (Teipel et al., 2009). Because our diagnostic groups displayed significant differences in age and education, we regressed out their effect on our variables of interest. Consistent with previous studies, the MCI A−N+ subjects of our report presented a less important proportion of APOE ε4 carriers than MCI A+N+ individuals (Jack et al., 2016b; Vos et al., 2013).

5. Conclusions

Using advanced image processing and network analysis techniques, we demonstrated that MCI subgroups display distinct patterns of alteration and can be differentiated using DTI and connectome analysis. Among MCI subgroups, only MCI A+N+ displayed an AD-like disconnection pattern suggesting that connectomic studies interested in prodromal AD may gain in specificity by enriching their sample with individuals who are positive for both amyloid and neurodegeneration. MCI A−N+ displayed a wider but weaker pattern of alteration supporting the hypothesis of a multiplicity of etiologies and a non-AD origin of these patients.

Disclosure statement

The authors have no actual or potential conflicts of interest.

Acknowledgements

This work was supported by the program *"Investissements d'avenir"* ANR-10-IAIHU-06 (*Agence Nationale de la Recherche-10-IA Agence* Institut Hospitalo-Universitaire-6). Olivier Colliot is supported by a "Contrat d'Interface Local" from Assistance Publique-Hôpitaux de Paris (AP-HP). Harald Hampel is supported by the AXA Research Fund, the Fondation Université Pierre et Marie Curie, and the *"Fondation pour la Recherche sur Alzheimer"*, Paris, France.

The sponsors of the study had no role in study design, data analysis or interpretation, writing or decision to submit the report for publication.

Appendix A. Supplementary data

Supplementary data associated with this article can be found, in the online version, at http://dx.doi.org/10.1016/j.neurobiolaging.2017.03.023.

References

Acosta-Cabronero, J., Williams, G.B., Pengas, G., Nestor, P.J., 2010. Absolute diffusivities define the landscape of white matter degeneration in Alzheimer's disease. Brain 133, 529–539.

Albert, M.S., DeKosky, S.T., Dickson, D., Dubois, B., Feldman, H.H., Fox, N.C., Gamst, A., Holtzman, D.M., Jagust, W.J., Petersen, R.C., Snyder, P.J., Carrillo, M.C., Thies, B., Phelps, C.H., 2011. The diagnosis of mild cognitive impairment due to Alzheimer's disease: recommendations from the National Institute on Aging-Alzheimer's Association workgroups on diagnostic guidelines for Alzheimer's disease. Alzheimers Dement. 7, 270–279.

Alexander, A.L., Hurley, S.A., Samsonov, A.A., Adluru, N., Hosseinbor, A.P., Mossahebi, P., Tromp, D.P.M., Zakszewski, E., Field, A.S., 2011. Characterization of cerebral white matter properties using quantitative magnetic resonance imaging stains. Brain Connect. 1, 423–446.

Avants, B.B., Epstein, C.L., Grossman, M., Gee, J.C., 2008. Symmetric diffeomorphic image registration with cross-correlation: evaluating automated labeling of elderly and neurodegenerative brain. Med. Image Anal. 12, 26–41.

Bartzokis, G., 2011. Alzheimer's disease as homeostatic responses to age-related myelin breakdown. Neurobiol. Aging 32, 1341–1371.

Bollobás, B., 1998. Modern Graph Theory, Graduate Texts in Mathematics. Springer, New York.

Braak, H., Braak, E., 1997. Frequency of stages of Alzheimer-related lesions in different age categories. Neurobiol. Aging 18, 351–357.

Braskie, M.N., Jahanshad, N., Stein, J.L., Barysheva, M., McMahon, K.L., de Zubicaray, G.I., Martin, N.G., Wright, M.J., Ringman, J.M., Toga, A.W., Thompson, P.M., 2011. Common Alzheimer's disease risk variant within the CLU gene affects white matter microstructure in young adults. J. Neurosci. 31, 6764–6770.

Caroli, A., Prestia, A., Galluzzi, S., Ferrari, C., van der Flier, W.M., Ossenkoppele, R., Van Berckel, B., Barkhof, F., Teunissen, C., Wall, A.E., Carter, S.F., Scholl, M., Choo, I.H., Grimmer, T., Redolfi, A., Nordberg, A., Scheltens, P., Drzezga, A., Frisoni, G.B. For the Alzheimer's Disease Neuroimaging Initiative, 2015. Mild cognitive impairment with suspected nonamyloid pathology (SNAP): prediction of progression. Neurology 84, 508–515.

Caso, F., Agosta, F., Mattavelli, D., Migliaccio, R., Canu, E., Magnani, G., Marcone, A., Copetti, M., Falautano, M., Comi, G., Falini, A., Filippi, M., 2015. White matter degeneration in atypical Alzheimer disease. Radiology 277, 162–172.

Cho, S., Metcalfe, A.W.S., Young, C.B., Ryali, S., Geary, D.C., Menon, V., 2012. Hippocampal–prefrontal engagement and dynamic causal interactions in the maturation of children's fact retrieval. J. Cogn. Neurosci. 24, 1849–1866.

Daianu, M., Dennis, E.L., Jahanshad, N., Nir, T.M., Toga, A.W., Jack, C.R., Weiner, M.W., Thompson, P.M., 2013a. Alzheimer's disease disrupts rich club organization in brain connectivity networks. Proc. IEEE Int. Symp. Biomed. Imaging 266–269.

Daianu, M., Jahanshad, N., Nir, T.M., Toga, A.W., Jack, C.R., Weiner, M.W., Thompson, P.M. Alzheimer's Disease Neuroimaging Initiative, 2013b. Breakdown of brain connectivity between normal aging and Alzheimer's disease: a structural *k* -core network analysis. Brain Connect. 3, 407–422.

Daitz, H.M., Powell, T.P., 1954. Studies of the connexions of the fornix system. J. Neurol. Neurosurg. Psychiatry 17, 75–82.

De Vico Fallani, F., Richiardi, J., Chavez, M., Achard, S., 2014. Graph analysis of functional brain networks: practical issues in translational neuroscience. Philos. Trans. R. Soc. B. Biol. Sci. 369.

Delano-Wood, L., Stricker Nikki, H., Sorg Scott, F., Nation Daniel, A., Jak Amy, J., Woods Steven, P., Libon David, J., Delis Dean, C., Frank Lawrence, R., Bondi Mark, W., 2012. Posterior cingulum white matter disruption and its associations with verbal memory and stroke risk in mild cognitive impairment. J. Alzheimers Dis. 29, 589–603.

Dubois, B., Feldman, H.H., Jacova, C., Hampel, H., Molinuevo, J.L., Blennow, K., DeKosky, S.T., Gauthier, S., Selkoe, D., Bateman, R., Cappa, S., Crutch, S., Engelborghs, S., Frisoni, G.B., Fox, N.C., Galasko, D., Habert, M.-O., Jicha, G.A., Nordberg, A., Pasquier, F., Rabinovici, G., Robert, P., Rowe, C., Salloway, S., Sarazin, M., Epelbaum, S., de Souza, L.C., Vellas, B., Visser, P.J., Schneider, L., Stern, Y., Scheltens, P., Cummings, J.L., 2014. Advancing research diagnostic criteria for Alzheimer's disease: the IWG-2 criteria. Lancet Neurol. 13, 614–629.

Edmonds, E.C., Delano-Wood, L., Galasko, D.R., Salmon, D.P., Bondi, M.W., 2015. Subtle cognitive decline and biomarker staging in preclinical Alzheimer's disease. J. Alzheimers Dis. 47, 231–242.

Eustache, P., Nemmi, F., Saint-Aubert, L., Pariente, J., Péran, P., 2016. Multimodal magnetic resonance imaging in Alzheimer's disease patients at prodromal stage. J. Alzheimers Dis. 50, 1035–1050.

Ferri, C.P., Prince, M., Brayne, C., Brodaty, H., Fratiglioni, L., Ganguli, M., Hall, K., Hasegawa, K., Hendrie, H., Huang, Y., Jorm, A., Mathers, C., Menezes, P.R., Rimmer, E., Scazufca, M. Alzheimer's Disease International, 2005. Global prevalence of dementia: a Delphi consensus study. Lancet Lond. Engl. 366, 2112–2117.

Fischer, F.U., Wolf, D., Scheurich, A., Fellgiebel, A., 2015. Altered whole-brain white matter networks in preclinical Alzheimer's disease. Neuroimage Clin. 8, 660–666.

Fischl, B., van der Kouwe, A., Destrieux, C., Halgren, E., Ségonne, F., Salat, D.H., Busa, E., Seidman, L.J., Goldstein, J., Kennedy, D., Caviness, V., Makris, N., Rosen, B., Dale, A.M., 2004. Automatically parcellating the human cerebral cortex. Cereb. Cortex 14, 11–22.

Gold, B.T., Zhu, Z., Brown, C.A., Andersen, A.H., LaDu, M.J., Tai, L., Jicha, G.A., Kryscio, R.J., Estus, S., Nelson, P.T., Scheff, S.W., Abner, E., Schmitt, F.A., Van Eldik, L.J., Smith, C.D., 2014. White matter integrity is associated with cerebrospinal fluid markers of Alzheimer's disease in normal adults. Neurobiol. Aging 35, 2263–2271.

Hagmann, P., Cammoun, L., Gigandet, X., Meuli, R., Honey, C.J., Wedeen, V.J., Sporns, O., 2008. Mapping the structural core of human cerebral cortex. PLoS Biol. 6, e159.

He, Y., Chen, Z., Evans, A., 2008. Structural insights into aberrant topological patterns of large-scale cortical networks in Alzheimer's disease. J. Neurosci. 28, 4756–4766.

Hof, P.R., Cox, K., Morrison, J.H., 1990. Quantitative analysis of a vulnerable subset of pyramidal neurons in Alzheimer's disease: I. Superior frontal and inferior temporal cortex. J. Comp. Neurol. 301, 44–54.

Hof, P.R., Morrison, J.H., 1991. Neocortical neuronal subpopulations labeled by a monoclonal antibody to calbindin exhibit differential vulnerability in Alzheimer's disease. Exp. Neurol. 111, 293–301.

Hua, K., Zhang, J., Wakana, S., Jiang, H., Li, X., Reich, D.S., Calabresi, P.A., Pekar, J.J., van Zijl, P.C.M., Mori, S., 2008. Tract probability maps in stereotaxic spaces: analyses of white matter anatomy and tract-specific quantification. NeuroImage 39, 336–347.

Jack, C.R., 2014. PART and SNAP. Acta Neuropathol. (Berl.) 128, 773–776.

Jack, C.R., Bennett, D.A., Blennow, K., Carrillo, M.C., Feldman, H.H., Frisoni, G.B., Hampel, H., Jagust, W.J., Johnson, K.A., Knopman, D.S., Petersen, R.C., Scheltens, P., Sperling, R.A., Dubois, B., 2016a. A/T/N: an unbiased descriptive

classification scheme for Alzheimer disease biomarkers. Neurology 87, 539–547.
Jack, C.R., Knopman, D.S., Chételat, G., Dickson, D., Fagan, A.M., Frisoni, G.B., Jagust, W., Mormino, E.C., Petersen, R.C., Sperling, R.A., van der Flier, W.M., Villemagne, V.L., Visser, P.J., Vos, S.J.B., 2016b. Suspected non-Alzheimer disease pathophysiology—concept and controversy. Nat. Rev. Neurol. 12, 117–124.
Jack, C.R., Knopman, D.S., Jagust, W.J., Petersen, R.C., Weiner, M.W., Aisen, P.S., Shaw, L.M., Vemuri, P., Wiste, H.J., Weigand, S.D., Lesnick, T.G., Pankratz, V.S., Donohue, M.C., Trojanowski, J.Q., 2013. Tracking pathophysiological processes in Alzheimer's disease: an updated hypothetical model of dynamic biomarkers. Lancet Neurol. 12, 207–216.
Jack, C.R., Knopman, D.S., Jagust, W.J., Shaw, L.M., Aisen, P.S., Weiner, M.W., Petersen, R.C., Trojanowski, J.Q., 2010. Hypothetical model of dynamic biomarkers of the Alzheimer's pathological cascade. Lancet Neurol. 9, 119–128.
Jack, C.R., Knopman, D.S., Weigand, S.D., Wiste, H.J., Vemuri, P., Lowe, V., Kantarci, K., Gunter, J.L., Senjem, M.L., Ivnik, R.J., Roberts, R.O., Rocca, W.A., Boeve, B.F., Petersen, R.C., 2012. An operational approach to National Institute on Aging-Alzheimer's Association criteria for preclinical Alzheimer disease. Ann. Neurol. 71, 765–775.
Jack, C.R., Therneau, T.M., Wiste, H.J., Weigand, S.D., Knopman, D.S., Lowe, V.J., Mielke, M.M., Vemuri, P., Roberts, R.O., Machulda, M.M., Senjem, M.L., Gunter, J.L., Rocca, W.A., Petersen, R.C., 2016c. Transition rates between amyloid and neurodegeneration biomarker states and to dementia: a population-based, longitudinal cohort study. Lancet Neurol. 15, 56–64.
Jack, C.R., Wiste, H.J., Weigand, S.D., Rocca, W.A., Knopman, D.S., Mielke, M.M., Lowe, V.J., Senjem, M.L., Gunter, J.L., Preboske, G.M., Pankratz, V.S., Vemuri, P., Petersen, R.C., 2014. Age-specific population frequencies of cerebral β-amyloidosis and neurodegeneration among people with normal cognitive function aged 50-89 years: a cross-sectional study. Lancet Neurol. 13, 997–1005.
Jahanshad, N., Zhan, L., Bernstein, M.A., Borowski, B.J., Jack, C.R., Toga, A.W., Thompson, P.M., 2010. Diffusion tensor imaging in seven minutes: determining trade-offs between spatial and directional resolution. Proc. IEEE Int. Symp. Biomed. Imaging 1161–1164.
Jeurissen, B., Tournier, J.-D., Dhollander, T., Connelly, A., Sijbers, J., 2014. Multi-tissue constrained spherical deconvolution for improved analysis of multi-shell diffusion MRI data. NeuroImage 103, 411–426.
Knopman, D.S., Jack, C.R., Lundt, E.S., Wiste, H.J., Weigand, S.D., Vemuri, P., Lowe, V.J., Kantarci, K., Gunter, J.L., Senjem, M.L., Mielke, M.M., Machulda, M.M., Roberts, R.O., Boeve, B.F., Jones, D.T., Petersen, R.C., 2015. Role of β-amyloidosis and neurodegeneration in subsequent imaging changes in mild cognitive impairment. JAMA Neurol. 72, 1475.
Knopman, D.S., Jack, C.R., Wiste, H.J., Weigand, S.D., Vemuri, P., Lowe, V., Kantarci, K., Gunter, J.L., Senjem, M.L., Ivnik, R.J., Roberts, R.O., Boeve, B.F., Petersen, R.C., 2012. Short-term clinical outcomes for stages of NIA-AA preclinical Alzheimer disease. Neurology 78, 1576–1582.
Knopman, D.S., Jack, C.R., Wiste, H.J., Weigand, S.D., Vemuri, P., Lowe, V.J., Kantarci, K., Gunter, J.L., Senjem, M.L., Mielke, M.M., Roberts, R.O., Boeve, B.F., Petersen, R.C., 2013. Brain injury biomarkers are not dependent on β-amyloid in normal elderly: neuronal injury biomarkers. Ann. Neurol. 73, 472–480.
Knowles, W.D., Schwartzkroin, P.A., 1981. Axonal ramifications of hippocampal Ca1 pyramidal cells. J. Neurosci. 1, 1236–1241.
Korolev, I.O., Symonds, L.L., Bozoki, A.C. Alzheimer's Disease Neuroimaging Initiative, 2016. Predicting progression from mild cognitive impairment to Alzheimer's dementia using clinical, MRI, and plasma biomarkers via probabilistic pattern classification. PLoS One 11, e0138866.
Kozlovskiy, S.A., Pyasik, M.M., Korotkova, A.V., Vartanov, A.V., Glozman, J.M., Kiselnikov, A.A., 2014. Activation of left lingual gyrus related to working memory for schematic faces. Int. J. Psychophysiol. 94, 241.
Landau, S.M., Mintun, M.A., Joshi, A.D., Koeppe, R.A., Petersen, R.C., Aisen, P.S., Weiner, M.W., Jagust, W.J. for the Alzheimer's Disease Neuroimaging Initiative, 2012. Amyloid deposition, hypometabolism, and longitudinal cognitive decline. Ann. Neurol. 72, 578–586.
Laxton, A.W., Tang-Wai, D.F., McAndrews, M.P., Zumsteg, D., Wennberg, R., Keren, R., Wherrett, J., Naglie, G., Hamani, C., Smith, G.S., Lozano, A.M., 2010. A phase I trial of deep brain stimulation of memory circuits in Alzheimer's disease. Ann. Neurol. 68, 521–534.
Leemans, A., Jones, D.K., 2009. The B-matrix must be rotated when correcting for subject motion in DTI data. Magn. Reson. Med. 61, 1336–1349.
Leow, A.D., Yanovsky, I., Chiang, M.-C., Lee, A.D., Klunder, A.D., Lu, A., Becker, J.T., Davis, S.W., Toga, A.W., Thompson, P.M., 2007. Statistical properties of Jacobian maps and the realization of unbiased large-deformation nonlinear image registration. IEEE Trans. Med. Imaging 26, 822–832.
Ma, X., Li, Z., Jing, B., Liu, H., Li, D., Li, H. Alzheimer's Disease Neuroimaging Initiative, 2016. Identify the atrophy of Alzheimer's disease, mild cognitive impairment and normal aging using morphometric MRI analysis. Front. Aging Neurosci. 8, 243.
Madhavan, A., Schwarz, C.G., Duffy, J.R., Strand, E.A., Machulda, M.M., Drubach, D.A., Kantarci, K., Przybelski, S.A., Reid, R.I., Senjem, M.L., Gunter, J.L., Apostolova, L.G., Lowe, V.J., Petersen, R.C., Jack, C.R., Josephs, K.A., Whitwell, J.L., 2015. Characterizing white matter tract degeneration in syndromic variants of Alzheimer's disease: a diffusion tensor imaging study. J. Alzheimers Dis. 49, 633–643.
Mallio, C.A., Schmidt, R., de Reus, M.A., Vernieri, F., Quintiliani, L., Curcio, G., Beomonte Zobel, B., Quattrocchi, C.C., van den Heuvel, M.P., 2015. Epicentral disruption of structural connectivity in Alzheimer's disease. CNS Neurosci. Ther. 21, 837–845.
Mayo, C.D., Mazerolle, E.L., Ritchie, L., Fisk, J.D., Gawryluk, J.R., 2017. Longitudinal changes in microstructural white matter metrics in Alzheimer's disease. Neuroimage Clin. 13, 330–338.
Meng, J.-Z., Guo, L.-W., Cheng, H., Chen, Y.-J., Fang, L., Qi, M., Jia, Z.-Y., Mohammed, W., Hong, X.-N., 2012. Correlation between cognitive function and the association fibers in patients with Alzheimer's disease using diffusion tensor imaging. J. Clin. Neurosci. 19, 1659–1663.
Metzler-Baddeley, C., Hunt, S., Jones, D.K., Leemans, A., Aggleton, J.P., O'Sullivan, M.J., 2012. Temporal association tracts and the breakdown of episodic memory in mild cognitive impairment. Neurology 79, 2233–2240.
Molinuevo, J.L., Ripolles, P., Simó, M., Lladó, A., Olives, J., Balasa, M., Antonell, A., Rodriguez-Fornells, A., Rami, L., 2014. White matter changes in preclinical Alzheimer's disease: a magnetic resonance imaging-diffusion tensor imaging study on cognitively normal older people with positive amyloid β protein 42 levels. Neurobiol. Aging 35, 2671–2680.
Mormino, E.C., Betensky, R.A., Hedden, T., Schultz, A.P., Amariglio, R.E., Rentz, D.M., Johnson, K.A., Sperling, R.A., 2014. Synergistic effect of β-amyloid and neurodegeneration on cognitive decline in clinically normal individuals. JAMA Neurol. 71, 1379–1385.
Morrison, J.H., Hof, P.R., 1997. Life and death of neurons in the aging brain. Science 278, 412–419.
Morrison, J.H., Hof, P.R., 2002. Selective vulnerability of corticocortical and hippocampal circuits in aging and Alzheimer's disease. Prog. Brain Res. 136, 467–486.
Nir, T., Jahanshad, N., Jack, C.R., Weiner, M.W., Toga, A.W., Thompson, P.M. the Alzheimer's Disease Neuroimaging Initiative (ADNI), 2012. Small world network measures predict white matter degeneration in patients with in patients with early-stage mild cognitive impairment. Proc. IEEE Int. Symp. Biomed. Imaging 1405–1408.
Nir, T.M., Jahanshad, N., Toga, A.W., Bernstein, M.A., Jack, C.R., Weiner, M.W., Thompson, P.M., 2015. Connectivity network measures predict volumetric atrophy in mild cognitive impairment. Neurobiol. Aging 36, S113–S120.
Nowrangi, M.A., Rosenberg, P.B., 2015. The fornix in mild cognitive impairment and Alzheimer's disease. Front. Aging Neurosci. 7, 1.
Oddo, S., Caccamo, A., Tran, L., Lambert, M.P., Glabe, C.G., Klein, W.L., LaFerla, F.M., 2006. Temporal profile of amyloid-beta (Abeta) oligomerization in an in vivo model of Alzheimer disease. A link between Abeta and tau pathology. J. Biol. Chem. 281, 1599–1604.
Petersen, R.C., 2011. Mild cognitive impairment. N. Engl. J. Med. 364, 2227–2234.
Petersen, R.C., Aisen, P., Boeve, B.F., Geda, Y.E., Ivnik, R.J., Knopman, D.S., Mielke, M., Pankratz, V.S., Roberts, R., Rocca, W.A., Weigand, S., Weiner, M., Wiste, H., Jack, C.R., 2013. Mild cognitive impairment due to Alzheimer disease in the community. Ann. Neurol. 74, 199–208.
Petersen, R.C., Roberts, R.O., Knopman, D.S., Boeve, B.F., Geda, Y.E., Ivnik, R.J., Smith, G.E., Jack, C.R., 2009. Mild cognitive impairment: ten years later. Arch. Neurol. 66, 1447–1455.
Poulin, S.P., Dautoff, R., Morris, J.C., Barrett, L.F., Dickerson, B.C., 2011. Amygdala atrophy is prominent in early Alzheimer's disease and relates to symptom severity. Psychiatry Res. Neuroimaging 194, 7–13.
Prescott, J.W., Guidon, A., Doraiswamy, P.M., Roy Choudhury, K., Liu, C., Petrella, J.R. for the Alzheimer's Disease Neuroimaging Initiative, 2014. The Alzheimer structural connectome: changes in cortical network topology with increased amyloid plaque burden. Radiology 273, 175–184.
Prestia, A., Caroli, A., van der Flier, W.M., Ossenkoppele, R., Van Berckel, B., Barkhof, F., Teunissen, C.E., Wall, A.E., Carter, S.F., Schöll, M., Choo, I.H., Nordberg, A., Scheltens, P., Frisoni, G.B., 2013. Prediction of dementia in MCI patients based on core diagnostic markers for Alzheimer disease. Neurology 80, 1048–1056.
Rubinov, M., Sporns, O., 2010. Complex network measures of brain connectivity: uses and interpretations. NeuroImage 52, 1059–1069.
Smith, R.E., Tournier, J.-D., Calamante, F., Connelly, A., 2013. SIFT: spherical-deconvolution informed filtering of tractograms. NeuroImage 67, 298–312.
Sporns, O., Tononi, G., Edelman, G.M., 2000. Theoretical neuroanatomy: relating anatomical and functional connectivity in graphs and cortical connection matrices. Cereb. Cortex 10, 127–141.
Tamamaki, N., Abe, K., Nojyo, Y., 1988. Three-dimensional analysis of the whole axonal arbors originating from single CA2 pyramidal neurons in the rat hippocampus with the aid of a computer graphic technique. Brain Res. 452, 255–272.
Teipel, S.J., Thomas, M., Maximilian, W., Thomas, K., Katharina, B., Reiser, M.F., Sabine, H., Hans-Jürgen, M., Harald, H., 2009. White matter microstructure in relation to education in aging and Alzheimer's disease. J. Alzheimers Dis. 17, 571–583.
Toledo, J.B., Weiner, M.W., Wolk, D.A., Da, X., Chen, K., Arnold, S.E., Jagust, W., Jack, C., Reiman, E.M., Davatzikos, C., Shaw, L.M., Trojanowski, J.Q. Alzheimer's Disease Neuroimaging Initiative, 2014. Neuronal injury biomarkers and prognosis in ADNI subjects with normal cognition. Acta Neuropathol. Commun. 2, 26.
Toledo, J.B., Zetterberg, H., van Harten, A.C., Glodzik, L., Martinez-Lage, P., Bocchio-Chiavetto, L., Rami, L., Hansson, O., Sperling, R., Engelborghs, S., Osorio, R.S., Vanderstichele, H., Vandijck, M., Hampel, H., Teipl, S., Moghekar, A., Albert, M., Hu, W.T., Monge Argilés, J.A., Gorostidi, A., Teunissen, C.E., De Deyn, P.P., Hyman, B.T., Molinuevo, J.L., Frisoni, G.B., Linazasoro, G., de Leon, M.J., van der Flier, W.M., Scheltens, P., Blennow, K., Shaw, L.M., Trojanowski, J.Q., 2015.

Alzheimer's disease cerebrospinal fluid biomarker in cognitively normal subjects. Brain 138, 2701–2715.
Tournier, J.-D., Calamante, F., Connelly, A., 2007. Robust determination of the fibre orientation distribution in diffusion MRI: non-negativity constrained super-resolved spherical deconvolution. NeuroImage 35, 1459–1472.
Tournier, J.-D., Calamante, F., Connelly, A., 2012. MRtrix: diffusion tractography in crossing fiber regions. Int. J. Imaging Syst. Technol. 22, 53–66.
Tustison, N.J., Avants, B.B., 2013. Explicit B-spline regularization in diffeomorphic image registration. Front. Neuroinformatics 7, 39.
Vos, S.J., Xiong, C., Visser, P.J., Jasielec, M.S., Hassenstab, J., Grant, E.A., Cairns, N.J., Morris, J.C., Holtzman, D.M., Fagan, A.M., 2013. Preclinical Alzheimer's disease and its outcome: a longitudinal cohort study. Lancet Neurol. 12, 957–965.
Vos, S.J.B., Gordon, B.A., Su, Y., Visser, P.J., Holtzman, D.M., Morris, J.C., Fagan, A.M., Benzinger, T.L.S., 2016. NIA-AA staging of preclinical Alzheimer disease: discordance and concordance of CSF and imaging biomarkers. Neurobiol. Aging 44, 1–8.
Vos, S.J.B., Verhey, F., Frölich, L., Kornhuber, J., Wiltfang, J., Maier, W., Peters, O., Rüther, E., Nobili, F., Morbelli, S., Frisoni, G.B., Drzezga, A., Didic, M., van Berckel, B.N.M., Simmons, A., Soininen, H., Kłoszewska, I., Mecocci, P., Tsolaki, M., Vellas, B., Lovestone, S., Muscio, C., Herukka, S.-K., Salmon, E., Bastin, C., Wallin, A., Nordlund, A., de Mendonça, A., Silva, D., Santana, I., Lemos, R., Engelborghs, S., Van der Mussele, S., The Alzheimer's Disease Neuroimaging Initiative, Freund-Levi, Y., Wallin, Å.K., Hampel, H., van der Flier, W., Scheltens, P., Visser, P.J., 2015. Prevalence and prognosis of Alzheimer's disease at the mild cognitive impairment stage. Brain 138, 1327–1338.
Wakana, S., Caprihan, A., Panzenboeck, M.M., Fallon, J.H., Perry, M., Gollub, R.L., Hua, K., Zhang, J., Jiang, H., Dubey, P., Blitz, A., van Zijl, P., Mori, S., 2007. Reproducibility of quantitative tractography methods applied to cerebral white matter. NeuroImage 36, 630–644.
Warren, J.D., Rohrer, J.D., Schott, J.M., Fox, N.C., Hardy, J., Rossor, M.N., 2013. Molecular nexopathies: a new paradigm of neurodegenerative disease. Trends Neurosci. 36, 561–569.
Wirth, M., Villeneuve, S., Haase, C.M., Madison, C.M., Oh, H., Landau, S.M., Rabinovici, G.D., Jagust, W.J., 2013. Associations between Alzheimer disease biomarkers, neurodegeneration, and cognition in cognitively normal older people. JAMA Neurol. 70, 1512–1519.
Wisse, L.E.M., Butala, N., Das, S.R., Davatzikos, C., Dickerson, B.C., Vaishnavi, S.N., Yushkevich, P.A., Wolk, D.A., 2015. Suspected non-AD pathology in mild cognitive impairment. Neurobiol. Aging 36, 3152–3162.
Yao, Z., Zhang, Y., Lin, L., Zhou, Y., Xu, C., Jiang, T. Alzheimer's Disease Neuroimaging Initiative, 2010. Abnormal cortical networks in mild cognitive impairment and Alzheimer's disease. Plos Comput. Biol. 6, e1001006.
Zalesky, A., Cocchi, L., Fornito, A., Murray, M.M., Bullmore, E., 2012. Connectivity differences in brain networks. NeuroImage 60, 1055–1062.
Zalesky, A., Fornito, A., Bullmore, E.T., 2010. Network-based statistic: identifying differences in brain networks. NeuroImage 53, 1197–1207.
Zhan, L., Jahanshad, N., Ennis, D.B., Jin, Y., Bernstein, M.A., Borowski, B.J., Jack, C.R., Toga, A.W., Leow, A.D., Thompson, P.M., 2013. Angular versus spatial resolution trade-offs for diffusion imaging under time constraints: angular versus spatial resolution trade-offs. Hum. Brain Mapp. 34, 2688–2706.
Zhu, Q.-Y., Bi, S.-W., Yao, X.-T., Ni, Z.-Y., Li, Y., Chen, B.-Y., Fan, G.-G., Shang, X.-L., 2015. Disruption of thalamic connectivity in Alzheimer's disease: a diffusion tensor imaging study. Metab. Brain Dis. 30, 1295–1308.